LAWRENCE
LIVERMORE
NATIONAL
LABORATORY

LLNL-JRNL-414365

Modeling Flow Past a Tilted Vena Cava Filter

M. A. Singer, S. L. Wang

June 30, 2009

Journal of Medical Devices

Disclaimer

Modeling Flow Past a Tilted Vena Cava Filter

Corresponding author:
Michael A. Singer
Center for Applied Scientific Computing
Lawrence Livermore National Laboratory
7000 East Avenue, L-550
Livermore, CA 95440
(925) 424-6529 (voice)
(925) 424-2477 (fax)
msinger@llnl.gov

Stephen L. Wang
Division of Vascular and Interventional Radiology
Kaiser Permanente

Modeling Flow Past a Tilted Vena Cava Filter

Michael A. Singer [a,*] and Stephen L. Wang [b]

[a] *Center for Applied Scientific Computing, Lawrence Livermore National Laboratory, Livermore, CA 94550, USA*

[b] *Division of Vascular and Interventional Radiology, Kaiser Permanente, Santa Clara Medical Center, Santa Clara, CA 95051, USA*

Abstract

Background. Inferior vena cava filters are medical devices used to prevent pulmonary embolism (PE) from deep vein thrombosis. In particular, retrievable filters are well-suited for patients who are unresponsive to anticoagulation therapy and whose risk of PE decreased with time. The goal of this work is to use computational fluid dynamics to evaluate the flow past an unoccluded and partially occluded Celect inferior vena cava filter. In particular, the hemodynamic response to thrombus volume and filter tilt is examined, and the results are compared with flow conditions that are known to be thrombogenic.

Methods. A computer model of the filter inside a model vena cava is constructed using high resolution digital photographs and methods of computer aided design. The models are parameterized using the Overture software framework, and a collection of overlapping grids is constructed to discretize the flow domain. The incompressible Navier-Stokes equations are solved, and the characteristics of the flow (i.e., velocity contours and wall shear stresses) are computed.

Results. The volume of stagnant and recirculating flow increases with thrombus volume. In addition, as the filter increases tilt, the cava wall adjacent to the tilted filter is subjected to low velocity flow that gives rise to regions of low wall shear stress.

Conclusions. The results demonstrate the ease of IVC filter modeling with the Overture software framework. Flow conditions caused by the tilted Celect filter may elevate the risk of intrafilter thrombosis and facilitate vascular remodeling. This latter condition also increases the risk of penetration and potential incorporation of the hook of the filter into the vena caval wall, thereby complicating filter retrieval. Consequently, severe tilt at the time of filter deployment may warrant early clinical intervention.

Keywords: Celect, CFD, Inferior vena cava, Overset grids, IVC filter

1 Introduction

Inferior vena cava (IVC) filters are a routine clinical treatment for the prevention of pulmonary embolism (PE) from deep vein thrombosis. In addition, IVC filters are used for prophylactic purposes in patients who are at high risk of developing pulmonary embolism. There are approximately eight different styles of IVC filters available in the United States, each with a unique filter design.

Permanent IVC filters (e.g., TrapEase [Cordis, Miami Lakes, FL], Greenfield [Boston Scientific, Boston, MA]) are designed to remain implanted in the patient. They are well-suited for patients who are unresponsive to medication and are at chronic risk of PE. In contrast, retrievable IVC filters (e.g., Günther Celect [Cook, Bloomington, IN], OptEase [Cordis, Miami Lakes, FL]) are designed to be removed following a temporary period of elevated risk of PE (e.g., trauma patients, combat soldiers); however, retrievable IVC filters do not have to be removed.

An ideal IVC filter causes minimal disruption to the flow, effectively traps deadly pulmonary emboli, is not inherently thrombogenic, is deployable by a low profile delivery system, and exhibits no long-term clinical complications. In working towards the construction of optimally designed filters, it is useful to examine clinical records for complications resulting from existing designs and to recognize that the optimal design may be patient-specific. One clinical complication that is especially troubling with retrievable filters is tilting of the device upon deployment. That is, filters are usually deployed so that the apex of the device is centered in the vessel and therefore traps thrombi in the center of the vein and away from the wall of the vessel. However, a filter may be tilted at deployment due to curvature within the cava (e.g., scoliosis), angulation of the vena cava or other factors. Tilted filters alter the hemodynamics within the IVC and complicate filter removal because the retrieval mechanism (usually a hook at the apex) may become embedded in the wall of the vessel.

High resolution computational fluid dynamics (CFD), coupled with realistic filter models, can characterize the hemodynamics of unoccluded and partially occluded non-tilted and tilted filters. In contrast to time consuming in-vitro experiments, different filter positions are tested without physically constructing and adjusting the device. In addition, physical quantities such as WSS and pressure gradients, which may be difficult to measure experimentally, can be computed precisely. As a result, computer modeling aids in our understanding of clinically relevant flow dynamics and is a tool for predicting and guiding clinical response.

* Corresponding author.
Email address: msinger@llnl.gov (Michael A. Singer).

There is precedence for computer modeling of IVC filters. In Swaminathan et al. [1], a finite element based CFD approach was used to examine the flow through an unoccluded stainless steel Greenfield vena cava filter. Here, a thin wire model represented the filter, and a straight pipe modeled the IVC. Results from the simulations, such as wall shear stress (WSS) and the identification of stagnation zones, were used to characterized the efficacy of the filter. The simulations also examined the filter's ability to trap clots. Non-Newtonian properties of blood had little impact on the flow field when compared to the Newtonian model. The work of Singer et al. [2] used CFD to study flow past an unoccluded and partially occluded TrapEase filter (Cordis, Miami Lakes, FL). That work examined flow patterns with different sizes, shapes, and locations of simulated thrombi. Spherical thrombi with larger volumes led to larger regions of stagnant and recirculating flow; WSS also increased with thrombus volume. Thrombus trapped in the upstream trapping position resulted in stagnant and recirculating flow along the cava wall, which may be thrombogenic. In all simulations, a standard TrapEase filter was modeled. Stewart et al. [3] also used CFD to model the hemodynamics past the TrapEase and two other unoccluded and partially occluded IVC filters. Their study examined the effects of IVC filters on blood flow, velocity patterns, and WSS; in-vitro studies were also performed.

Extensive in-vitro tests have also been performed on IVC filters. In addition to the work of Stewart et al. [3], Leask et al. [4,5] studied the hemodynamics of unoccluded and partially occluded Simon nitinol (NMT Medical, Woburn, MA) and TrapEase filters. Using a photochromic grid method [6], velocity contours and wall shear stresses were computed. For both filters, model thrombus caused significant disruption to the flow and increased the WSS.

In all of the studies described above, flow was examined past a tilt-free filter. In contrast, the present work uses CFD to examine the flow past an upright and tilted Celect filter, which is both unoccluded and partially occluded. In particular, the question to be addressed is: Is the Celect filter more thrombogenic in the tilted position than in the upright position? That is, does the tilted filter lead to hemodynamic conditions (e.g., stagnant and recirculating flow, abnormal WSS) that may promote intrafilter thrombosis? These are important clinical questions whose answers may dictate a particular clinical response (e.g., no response, filter retrieval, thrombolytics). In addition, hemodynamic conditions near the hook of the filter may dictate its susceptibility to become embedded in the vessel wall thereby complicating filter retrieval. Following Singer et al. [2], the present work uses a finite difference based method of overlapping grids to examine flow past the unoccluded and partially occluded Celect. The IVC is modeled as a straight tube, and a three-dimensional geometric model of the Celect is constructed using high resolution digital photographs and methods of computer aided design. Flow dynamics are characterized by velocity contours and wall shear stresses.

(a)  (b) 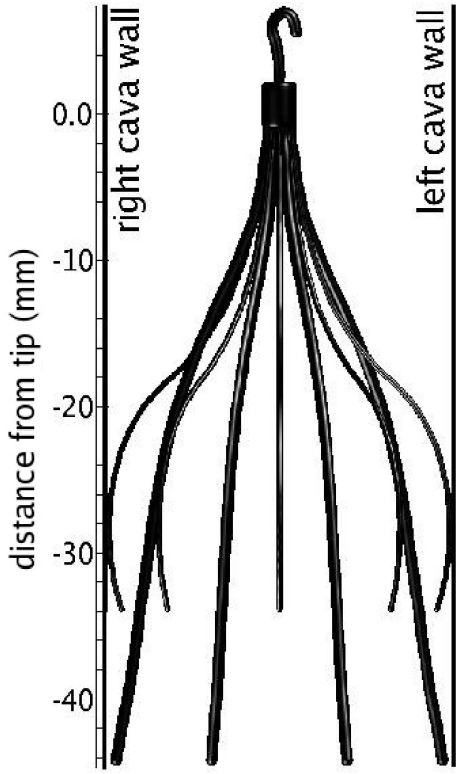

Fig. 1. Celect filter: (a) real filter in a glass test tube with a 23 mm inner diameter; (b) three-dimensional computer model sized to fit the same tube. Note the labeling of the radiological right and left walls of the cava.

2 Methods

The Celect IVC filter (Fig. 1) is a low profile, asymmetric, retrievable, nitinol filter that is manufactured by Cook Medical (Bloomington, IN). The design of the Celect follows that of Cook's Günther Tulip filter, and the Celect has been retrieved from patients after being implanted for more than one year [7]. Patients whose risk of pulmonary embolism decreases with time may be candidates for retrievable filters such as the Celect. Fig. 1a shows the real filter deployed in a glass test tube with an inner diameter of 23 mm; Fig. 1b is the corresponding computer model.

The hook attached to the top of the filter allows retrieval of the Celect via a sheath inserted into the jugular vein. Fastening hooks at the end of the four straight legs (Fig. 1a) attach to the IVC and hold the filter in-place. The remaining eight curved legs are designed to support the filter and keep it centered in the vessel.

The IVC is modeled as a straight, rigid tube with an inner diameter of 23 mm, per the average cava diameter described in Kaufman et al. [8]. The length of the tube is 104 mm, which provides adequate distance for the inlet velocity profile to develop fully before reaching the filter. Two overlapping grids are used to discretize the interior of the IVC: one high-resolution grid covers the inner boundary adjacent to the wall of the tube, and a second low-resolution grid fills the interior of the tube. By using a high-resolution grid near the boundary, adequate resolution of the boundary layer is ensured.

A rigid, three-dimensional model of the Celect filter is constructed using the computer aided design features of the Overture software framework [9]. The starting point for developing the model is a set of high-resolution digital photographs (e.g., Fig. 1a) that capture the compressed filter in a glass test tube with a 23 mm inner diameter (the same diameter as the model cava). The photographs are then imported into the GNU Image Manipulation Package where the filter geometry is extracted from pixel color and coordinates. The data are then imported into Overture where the geometry is parameterized and a mesh of the filter is constructed. Additional measurements of the filter (e.g., leg and tip sizes) are obtained using a digital caliper. The filter is discretized using approximately 50 body-fitted, overlapping grids. The spatial resolution of the grids is adjustable and is chosen to ensure adequate resolution of the flow throughout the entire domain (see study of spatial convergence below). The final computer model of the Celect filter is shown in Fig. 1b. Note that the model does not include the fastening hooks, which fasten the Celect to the vein. Once deployed, these hooks become embedded in the vein and therefore do not obstruct the flow.

Thrombi are modeled as rigid spheres of 0.5mL and 1mL, which are representative of the volumes studied in-vitro by Wang et al. [10]. In-vivo clots often assume random shapes with variable elasticity and porosity, but as noted by Swaminathan et al. [1], spherical models represent, in some sense, a statistical average of irregular shapes.

2.2 Governing equations and parameters

Blood is modeled as a homogeneous, incompressible, Newtonian fluid with density $\rho = 1040$ kg/m^3 and a dynamic viscosity $\mu = 2.57 \times 10^{-3}$ kg/(ms). From the work of Swaminathan et al. [1], the Newtonian approximation is appropriate for the current flow regime: non-Newtonian effects are minimal. The flow obeys conservation of mass and momentum as described by the

incompressible Navier-Stokes (NS) equations [11],

$$\nabla \cdot \mathbf{u} = 0, \tag{1}$$

$$\rho\left(\frac{\partial \mathbf{u}}{\partial t} + \mathbf{u} \cdot \nabla \mathbf{u}\right) = -\nabla p + \nabla \cdot \left(\mu(\nabla \mathbf{u} + (\nabla \mathbf{u}^{\mathrm{T}})\right). \tag{2}$$

Here, t is time, $\mathbf{u}$ is the velocity vector, p is the dynamic pressure, $\nabla \mathbf{u}$ is the velocity gradient tensor, and $(\nabla \mathbf{u})^{\mathrm{T}}$ is the transpose of $\nabla \mathbf{u}$. For the present work, the flow is taken to be steady, and all external forces (e.g., gravity) are ignored.

The single non-dimensional parameter that characterizes the flow is the Reynolds number, $\mathrm{Re} = \rho U D/\mu$. Here, U is the mean inlet velocity, and D is the diameter of the tube.

2.3 Discretization

The three-dimensional NS equations are solved using the incompressible flow solver, cgins, that is built upon the Overture software framework [12]. Overture uses the method of overset grids to discretize partial differential equations on a collection of curvilinear meshes using finite difference approximations [13]. In particular, cgins solves the velocity-pressure form of the NS equations, which are given by

$$\rho\left(\frac{\partial \mathbf{u}}{\partial t} + \mathbf{u} \cdot \nabla \mathbf{u}\right) = -\nabla p + \nabla \cdot \left(\mu(\nabla \mathbf{u} + (\nabla \mathbf{u}^{\mathrm{T}})\right), \tag{3}$$

$$\Delta p + \nabla \mathbf{u} : \nabla \mathbf{u} - \alpha \nabla \cdot \mathbf{u} = 0. \tag{4}$$

Here, the momentum equation is the same as equation (2), and the pressure equation is obtained by taking the divergence of the momentum equation and using the continuity equation (1). Note that the $\alpha \nabla \cdot \mathbf{u}$ term in the pressure equation helps ensure a divergence-free velocity (see [14] for details), and the size of α is proportional to the inverse of the square of the grid spacing. Equations (3)-(4), with appropriate boundary and initial conditions, are mathematically equivalent to equations (1)-(2)[14]. As discussed in [14], the velocity-pressure form of the equations requires an additional boundary condition, such as $\nabla \cdot \mathbf{u} = 0$, to guarantee the equivalence with the velocity-divergence formulation given in equations (1)-(2); this divergence-free condition on the velocity serves as a boundary condition for the Poisson equation for the pressure, as given in equation (4). By discretizing the velocity-pressure form of the equations with a compact scheme for Δp, one avoids the pressure

oscillations that may otherwise result when the velocity and pressure are co-located at grid points. Alternative approaches based on staggered grids are difficult to implement on general three-dimensional curvilinear grids.

This work uses second-order accurate spatial approximations, and the steady-state solution is computed using an implicit method based on line solves and the solution of tridiagonal systems. Artificial diffusion, based on second- and fourth-order undivided differences, is also used. The diffusion terms are added to the momentum equation to improve stability and do not impact the order of accuracy of the method.

2.4 Boundary conditions

The walls of the pipe are rigid, no-slip ($\mathbf{u} = 0$) boundaries, and the inflow is specified by a parabolic inlet velocity with the axial component having a prescribed peak velocity; the transverse velocity components are zero. The normal derivative of the pressure is zero at the inflow boundary. A mixed (Robin) condition on the pressure and an extrapolation on the velocity are used at the outflow. This approach allows waves to exit the domain smoothly and assumes the outflow boundary is far enough downstream so that the impact of this artificial condition is small. Indeed, the outflow boundary has minimal impact on the results below. The solid walls defining the surface of the filter are also modeled as rigid, no-slip boundaries.

All of the results presented here use a mean inlet velocity of $U = 3.87$ cm/s corresponding to Re = 360. Previously published reports of vena cava simulations (e.g., [3,16]) used similar Reynolds numbers. This Reynolds number corresponds to a blood flow rate of 0.96 L/min in a 2.3 cm vena cava, which is well within the range of 1.2 ± 0.5 L/min reported by Cheng et al. [17] for infrarenal flow at rest.

3 Results

The three-dimensional NS equations are solved to determine the three components of velocity and the pressure. In all of the figures below, the flow is bottom-to-top. Flow is modeled past the filter in three configurations: zero-tilt, where the tip of the filter is centered in the vein; half-tilt, where the tip is mid-way between the center and the wall of the vein; and full-tilt, where the hook on the tip is touching the wall of the vein. All three configurations are representative of clinical observations. The Celect is ideally positioned in the zero-tilt configuration.

The results below focus on the axial component of velocity, which is the dominant component. All wall shear stresses are plotted along two walls on opposite sides of the vessel and are in the plane of the tilted filter: the right cava wall, which is opposite the direction of tilt; and the left cava wall, which is in the direction of tilt. Note the use of the radiological right and left, as illustrated in Fig. 1b. These two locations are chosen because they represent the extremes of WSS variations experienced by the vessel. That is, as the filter tilts, the right wall becomes the farthest wall from the filter tip, while the left wall becomes the closest. Note that the abscissa of the WSS figures measures the distance from the tip of the filter (in the zero-tilt configuration); refer to Fig. 1b for a physical interpretation of the distance in relation to the filter. All velocities and wall shear stresses are normalized by the corresponding theoretical value for fully-developed flow in a long, straight pipe without a filter (i.e., Poiseuille flow).

3.1 Spatial convergence

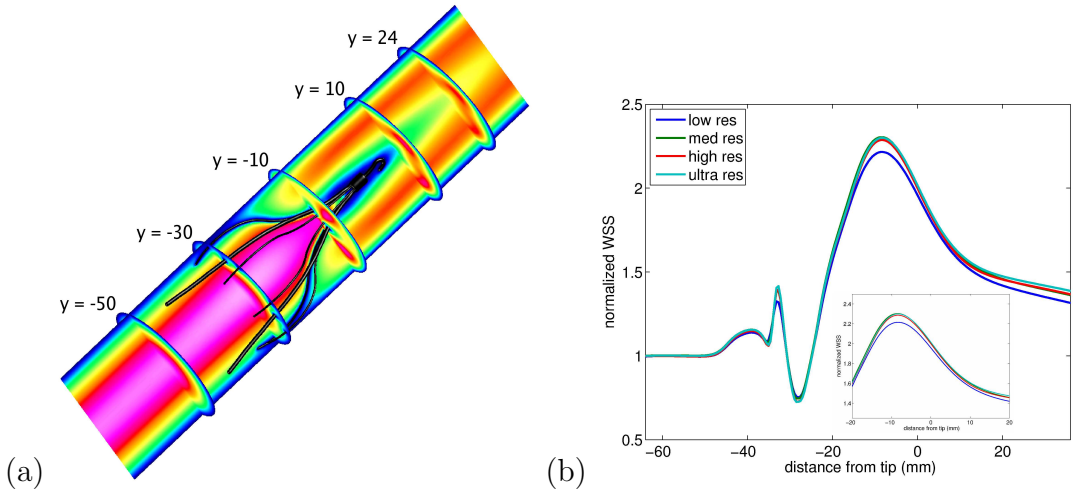

Fig. 2. A grid refinement study ensures sufficient spatial resolution: (a) slices at which spatial convergence (of axial velocity) is tested; (b) demonstration of wall shear stress convergence at $y = 24$, which is the location of greatest variation with grid resolution.

To ensure adequate spatial resolution, flow past the unoccluded filter is simulated using four grid resolutions: low (6.6M grid points), medium (8.4M grid points), high (10.5M grid points), and ultra (12.4M grid points). Velocity profiles are examined at five cross-stream locations in the flow (Fig. 2a), which include upstream, mid-filter, and downstream locations. In addition, the WSS is examined to ensure that the viscous boundary layer is resolved completely. Fig. 2b shows a representative plot of the normalized WSS versus axial distance for the four grid resolutions; the inset plot highlights the results near the peak WSS, where the impact of grid resolution is greatest. As demonstrated,

the normalized WSS profiles (and velocity profiles, which are not shown) converge with grid refinement, and the numerical results using the medium, high, and ultra resolutions are virtually identical.

resolution	grid points	L_∞ %-error – axial velocity	L_∞ %-error – WSS
low	6.6M	2.68	4.21
medium	8.4M	1.48	1.18
high	10.5M	0.32	0.97
ultra	12.4M	—	—

Table 1
Spatial convergence of the axial velocity and wall shear stress. The solutions obtained using the ultra grid resolution are taken to be the "exact" solutions.

Table 1 provides a quantitative demonstration of spatial convergence. Here, the L_∞ percent errors for the axial velocity and the WSS are computed relative to the solutions using the ultra grid resolution: solutions obtained on the ultra grid resolution are taken to be "exact". Similar results are observed for the L_2 errors. The table demonstrates that solutions obtained on the medium grid resolution are less than 1.5% different than the corresponding results from the ultra resolution grid. Consequently, the medium grid resolution is used for all subsequent simulations since it provides sufficient spatial resolution at a reasonable computational expense.

3.2 Unoccluded filter

Contour plots of the axial velocity are shown in Fig. 3. In all cases, the flow that enters the filter is fully developed. Flow with zero velocity is observed adjacent to all solid boundaries (i.e., vessel walls and filter), as expected from the no-slip boundary condition. Flow past the zero-tilt filter is nearly symmetric, with a region of low velocity flow surrounding the filter hook. With increasing tilt, flow symmetry is broken, and the volume of stagnant flow surrounding the filter hook increases due to a larger filter cross-section that is exposed to on-coming flow. For the case of full-tilt, a large region of stagnant flow is observed near the wall of the vessel, and low velocity flow is observed between the hook and the leg that touches the vein. These regions of slow flow lead to relatively long particle residence times, which may promote the accumulation of platelets. The peak normalized velocity, which occurs inside to the filter, also increases with filter tilt, but the minimum velocities remain virtually unchanged.

The WSS for the right and left cava walls becomes increasingly different with filter tilt (Fig. 4). On the right wall, the peak WSS decreases with filter tilt

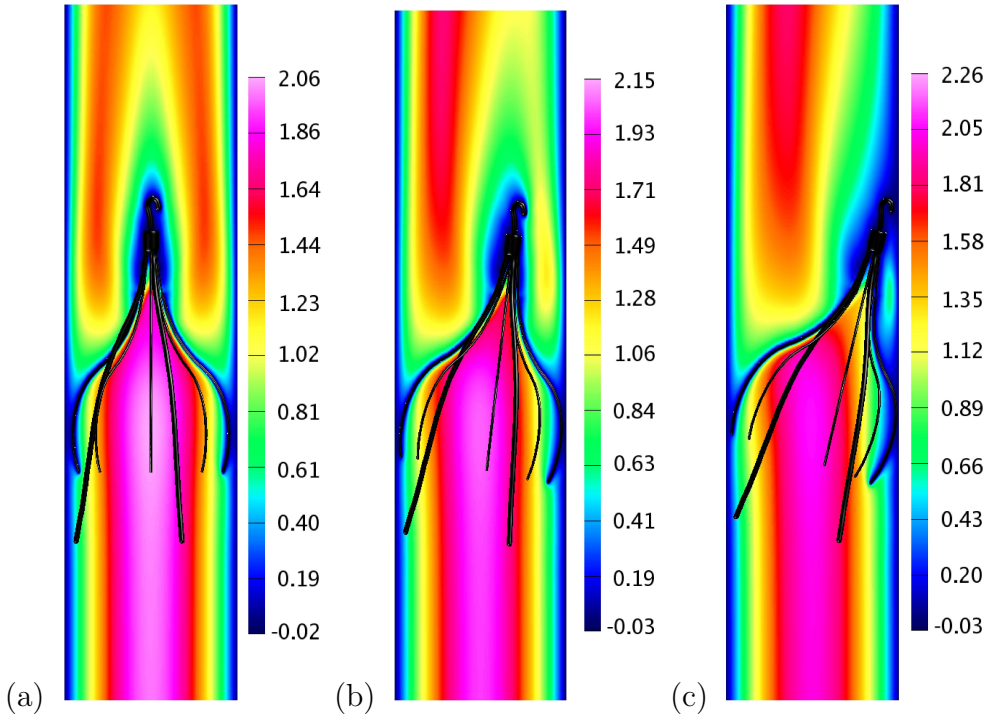

Fig. 3. Axial velocity contours for the unoccluded Celect filter: (a) zero-tilt; (b) half-tilt; (c) full-tilt.

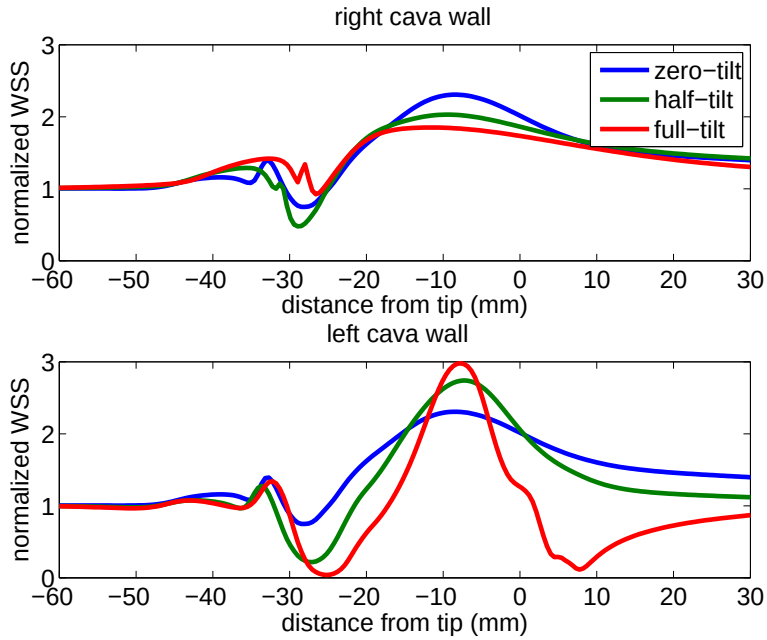

Fig. 4. Wall shear stress for the unoccluded Celect filter: right cava wall (top); left cava wall (bottom).

as the apex of the filter moves away from the wall and allows flow to pass through a wider opening thereby weakening the velocity gradient near the wall. Upstream of peak, the WSS drops below the free-stream value due to

momentum loss caused by the filter leg near the wall. The WSS nearly returns to its free-stream value at the outflow.

The left cava wall experiences flow disruption due to filter tilt (Fig. 4). As tilt increases, so does the peak WSS, which is located between the hook and leg/wall intersection. For the case of full-tilt, the flow immediately upstream and downstream of the hook is nearly stagnant (i.e., Fig. 3c), which leads to near zero WSS. These two regions of low WSS, which become more pronounced with tilt, may facilitate the accumulation of platelets. In addition, the close proximity of the hook to the cava wall elevates the risk of cava damage (e.g., perforation [18]), which further increases the risk of thrombosis.

3.3 Partially occluded filter

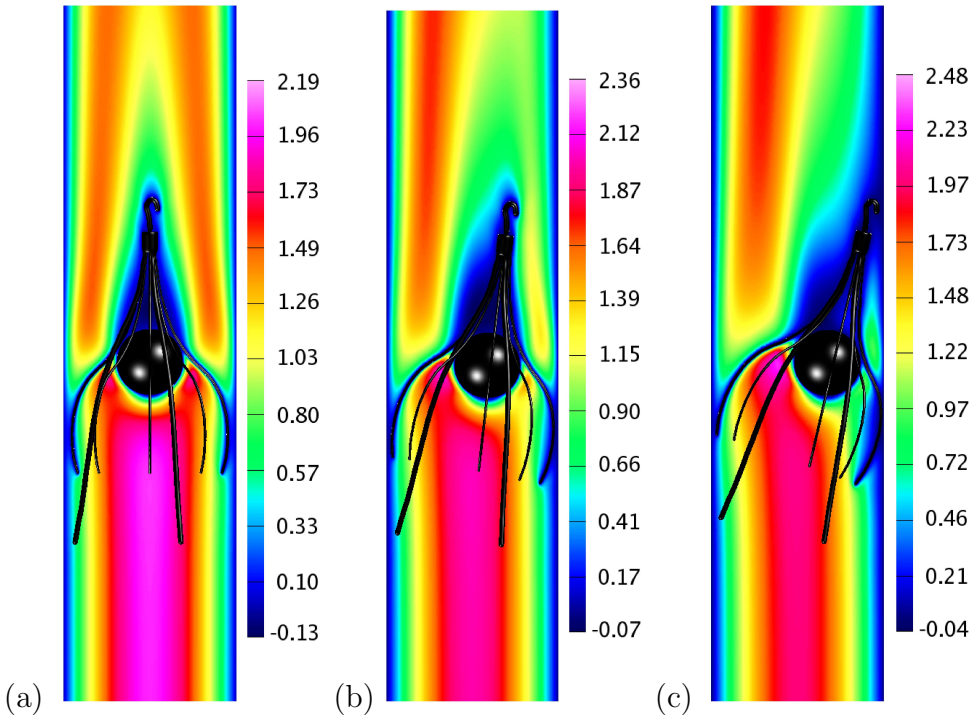

Fig. 5. Axial velocity contours for the partially occluded Celect filter with a 0.5mL spherical clot: (a) zero-tilt; (b) half-tilt; (c) full-tilt.

Flow past the partially occluded Celect with 0.5mL and 1mL spherical thrombus is shown in Fig. 5 and Fig. 6, respectively. In both cases, the zero-tilt configuration exhibits stagnant flow downstream of the thrombus and hook, and the disrupted flow is confined to the center of the vessel. As tilt and thrombus size increase, however, the volume of disrupted flow also increases, and a region of stagnant flow develops along the wall of the vessel. For the 1mL thrombus with full-tilt, flow disruption along the vessel wall persists well downstream of the filter, thereby providing hemodynamic conditions that may

be thrombogenic. Maximum axial velocities increase with tilt and thrombus volume; the minimum axial velocities also increase, which indicates a decrease in the strength of flow reversal as flow is pushed around the thrombus with greater velocity.

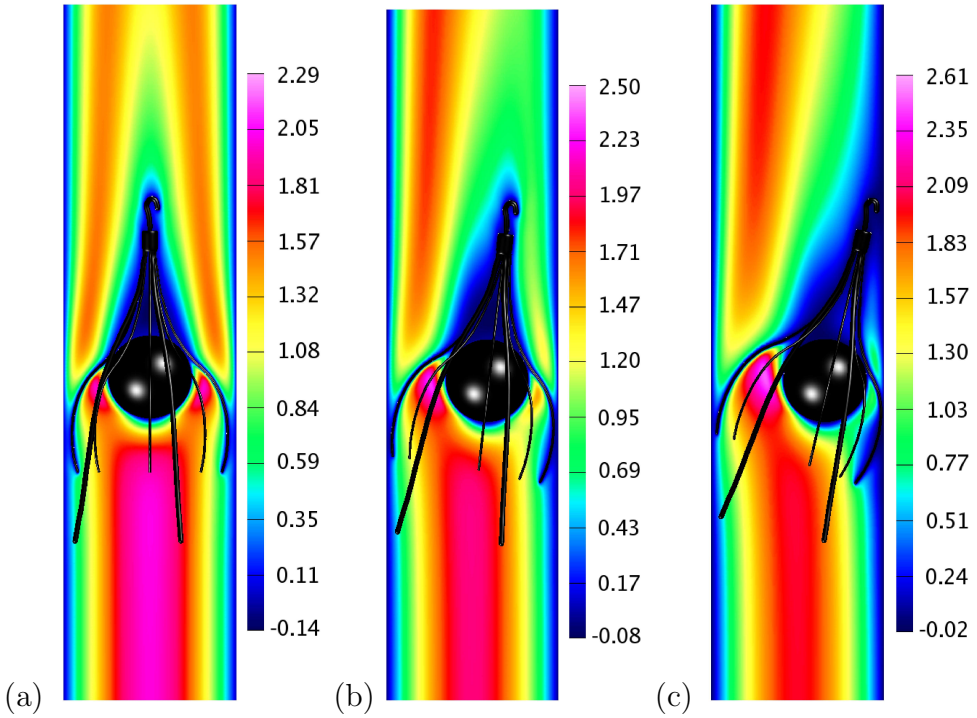

Fig. 6. Axial velocity contours for the partially occluded Celect filter with a 1mL spherical clot: (a) zero-tilt; (b) half-tilt; (c) full-tilt.

The peak WSS along the right cava wall decreases with filter tilt and increases with thrombus volume (Figs. 7 and 8). The former trend is due to a widening gap between the vessel wall and the clot, which results in lower velocity gradients in the boundary layer. Conversely, the larger thrombus provides a narrower passage between the vessel wall and the thrombus, which results in higher flow velocities past the thrombus in order to maintain conservation of mass. For both volumes of thrombus, a decrease in WSS is observed near the upstream contact point of the filter leg and vessel wall; this is a region of low velocity flow. In all cases, the WSS far downstream of the filter nearly returns to its unperturbed upstream value, which indicates that the disruption of the WSS due to the filter is localized.

Wall shear stress profiles for both thrombi are qualitatively similar. However, the magnitudes of the peak WSS increases with volume (similarly for axial velocity), while the minimum wall shear stresses remain virtually identical. In addition, the length of the left cava wall that is exposed to low normalized WSS (e.g., < 1) increases with tilt (both upstream and downstream of peak), but remains nearly constant for both sizes of thrombus.

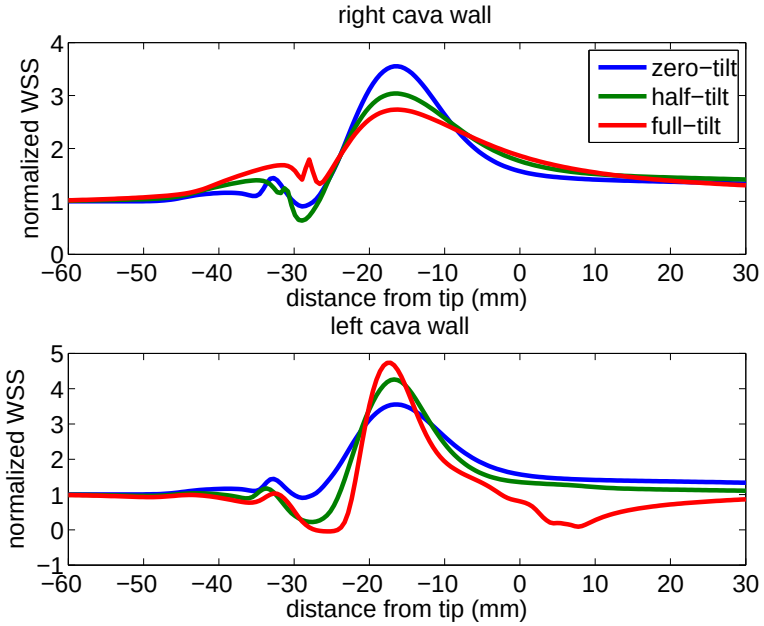

Fig. 7. Wall shear stress for the partially occluded Celect filter with 0.5mL thrombus: right cava wall (top); left cava wall (bottom).

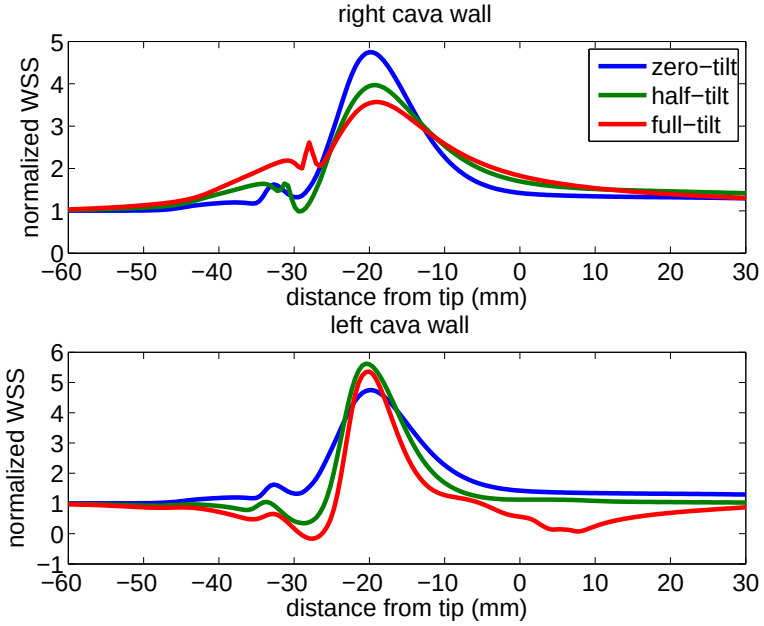

Fig. 8. Wall shear stress for the partially occluded Celect filter with 1mL thrombus: right cava wall (top); left cava wall (bottom).

4 Discussion

Stagnant and recirculating flow are thought to be thrombogenic due to platelet deposition [5,19–21]. Consequently, IVC filters that minimize disruption to

otherwise natural flow are less likely to promote thrombosis, which may lead to vessel occlusion. For the flow regime considered here, undisturbed flow (without a filter) is Poiseuille flow, which produces a parabolic velocity profile in the axial direction; all other velocity components are zero.

Retrievable filters that demonstrate excessive tilt are difficult to remove. In [22], for example, 390 patients received retrievable filters (Günther Tulip, OptEase, Recovery [Bard Peripheral Vascular, Tempe, AZ], Celect, and G2 [Bard Peripheral Vascular, Tempe, AZ]) at the Massachusetts General Hospital from May 2001 to July 2008. Of the 60/390 (15.4%) patients on whom retrieval was attempted, 45/60 (75%) filters were retrieved successively. For the 15 (25%) filters not retrieved, 4/15 (27%) were due to thrombus in the filter, 7/15 (47%) were due to incorporation of the filter legs into the IVC wall, 2/15 (13%) were due to the hook becoming embedded in the IVC wall, and 2/15 (13%) were due to significant filter tilt. Other clinical studies have also reported difficulty with filter retrieval – including the Celect – due to excessive intrafilter thrombus and tilt (e.g., [7,23,24]). Hence, a detailed understanding of the hemodynamics surrounding upright/tilted retrievable filters that are unoccluded and partially occluded is critical to predicting the potential success of retrieval.

The figures above indicate that the volume of stagnant and recirculating flow increases with tilt and thrombus volume. In particular, low velocity flow is observed near the apex of the filter (e.g., tip and hook) and immediately downstream of all thrombi. For the zero-tilt configuration, these abnormal flow patterns are located in the center of the vessel and away from the vessel walls. As tilt increases, however, the tip and hook of the filter move closer to the vessel wall, which exposes the vessel to slow flow with a longer residence time than the zero-tilt configuration. Consequently, the wall adjacent to the tilted filter is prone to platelet deposition and accumulation, and the risk of thrombosis increases, especially for the partially occluded filter. Further, as the volume of slow flow increases for the tilted, partially occluded filter, mass conservation (for a given cross section) is maintained by transferring momentum to other velocity components and by increasing the flow velocity in other parts of the vessel. As a result, this multi-directional, high velocity flow serves to prevent platelet aggregation and accumulation (and therefore thrombosis), but may also lead to sustained wall shear stresses that can damage the vessel or lead to vascular remodeling [25].

The formation of intimal hyperplasia and the remodeling of smooth muscle cells are linked to regions of low WSS and high WSS gradients [26,27]. Consequently, an IVC filter that promotes these hemodynamic effects, especially when tilted, is more likely to facilitate clinical complications that may require endovascular treatment. As observed above, when the Celect is fully tilted, it induces regions of low WSS along the left cava wall near the tip and hook of the filter; the length of cava wall that is exposed to low WSS increases with

thrombus volume. These regions of vessel are therefore at elevated risk of abnormal migration and growth of smooth muscle cells, which may ultimately lead to vessel occlusion. In addition, the close proximity of the tip/hook to the cava wall also raises the risk of vascular remodeling and vessel damage, especially if the hook becomes embedded in the vessel [18]. This latter condition also complicates filter retrieval for the Celect and other filters of similar design (e.g., Günther Tulip) [23,28].

Dissolution of thrombi increases with WSS [3]. That is, when wall shear stresses are sufficiently high, trapped thrombus are subjected to shear stresses that reduce thrombus volume by thrombolysis. As the Celect filter increases tilt, thrombi are trapped closer to the vessel wall, and the flow pattern is reminiscent of a TrapEase filter with thrombus in the upstream trapping position (i.e., thrombus trapped between the filter and cava wall) [2]. Consequently, the stagnant/recirculating zones and corresponding regions of low WSS retard dissolution and, as noted by Stewart et al., may promote continued aggregation of blood elements, clot growth, and intimal hyperplasia [3]. As noted by other computational and in-vitro studies [2–4,19], capturing thrombus next to the cava wall is not optimal and should be avoided. Hence, severely tilted filters that will trap thrombus against the cava wall may need to be recaptured at the time of deployment (before the filter is released).

5 Conclusions

Computational fluid dynamics is used to model flow through a Celect inferior vena cava filter. Studies are performed on both an unoccluded and partially occluded filter that is upright and tilted. Three-dimensional models of the filter are constructed from high resolution digital images, and the vena cava is modeled as a straight pipe. The computational domain is discretized using approximately 50 body-fitted overlapping grids, and the incompressible Navier-Stokes equations are solved using the Overture software framework.

Partial filter occlusion produces stagnant/recirculating flow, which increases with thrombus volume, downstream of the thrombus. As tilt increases, these regions of low velocity flow approach the vessel wall and give rise to low wall shear stresses near the apex of the filter. Consequently, the risk of thrombosis and cava occlusion, due to hemodynamic conditions known to produce such responses, increases with thrombus volume and filter tilt. Further, tilted filters increase the risk of cava penetration and complicate filter retrieval. As a result, severe tilt at the time of deployment may warrant early intervention, though further clinical studies that compare intrafilter and cava thrombosis rates among tilted and non-tilted filters should be pursued.

Acknowledgements

MAS is grateful for the assistance of Dr. William Henshaw. Computer time on LLNL's Yana cluster was provided under Livermore Computing's Multiprogrammatic & Institutional Computing Initiative. LLNL is operated by Lawrence Livermore National Security, LLC, for the DOE, National Nuclear Security Administration under Contract DE-AC52-07NA27344.

References

[1] Swaminathan, T.N., Hu, H.H., and Patel, A.A., 2006, "Numerical Analysis of the Hemodynamics and Embolus Capture of a Greenfield Vena Cava Filter," J. Biomed. Eng., 128, pp. 360-370.

[2] Singer, M.A., Henshaw, W.D., and Wang, S.L., 2009, "Computational Modeling of Blood Flow in the TrapEase Inferior Vena Cava Filter," J. Vasc. Interv. Radiol., 20, pp. 799-805.

[3] Stewart, S.F., Robinson, R.A., Nelson, R.A., and Malinauskas, R.A., 2008, "Effects of Thrombosed Vena Cava Filters on Blood Flow: Flow Visualization and Numerical Modeling," Ann. Biomed. Eng., 36(11), pp. 1764-1782.

[4] Leask, R.L., Johnston, K.W., and Ojha, M., 2001, "In Vitro Hemodynamic Evaluation of a Simon Nitinol Vena Cava Filter: Possible Explanation of IVC Occlusion," J. Vasc. Interv. Radiol., 12, pp. 613-618.

[5] Leask, R.L., Johnston, K.W., and Ojha, M., 2004, "Hemodynamic Effects of Clot Entrapment in the TrapEase Inferior Vena Cava Filter," J. Vasc. Intervent. Radiol., 15, pp. 485-490.

[6] Couch, G.G., Johnston, K.W., and Ojha, M., 1996, "Full-Field Visualization and Velocity Measurement With a Photochromic Grid Method," Meas. Sci. Technol., 7, pp. 1238-1246.

[7] Doody, O., Noë, G., Given, M.F., Foley, P.T., and Lyon, S.M., 2009, "Assessment of Snared-Loop Technique when Standard Retrieval of Inferior Vena Cava Filters Fails," Cardiovasc. Intervent. Radiol., 32(1), pp. 145-149.

[8] Kaufman, J.A., Waltman, A.C., Rivitz, S.M., and Geller, S.C., 1995, "Anatomical Observations on the Renal Veins and Inferior Vena Cava at Magnetic Resonance Angiography," Cardiovasc. Intervent. Radiol., 18, pp. 153-157.

[9] https://computation.llnl.gov/casc/Overture/

[10] Wang, S.L., Timmermans, H.A., and Kaufman, J.A., 2007, "Estimation of Trapped Thrombus Volumes in Retrievable Inferior Vena Cava Filters: A Visual Scale," J. Vasc. Interv. Radiol., 18, pp. 273-276.

[11] Batchelor, G.K., 1980, An Introduction to Fluid Dynamics, Cambridge University Press, Cambridge, UK.

[12] Henshaw, W.D., 2008, "Cgins: A Solver for the Incompressible Navier-Stokes Equations on Composite Overlapping Girds," LLNL Technical Report, LLNL-SM-403631.

[13] Chesshire, G.S., and Henshaw, W.D., 1990, "Composite Overlapping Meshes for the Solution of Partial Differential Equations," J. Comp. Phys., 90(1), pp. 1-64.

[14] Henshaw, W.D., 1994. "A Fourth-Order Accurate Method for the Incompressible Navier-Stokes Equations on Overlapping Grids," J. Comp. Phys., 113(1), pp. 13-25.

[15] Henshaw, W.D., and Petersson, N.A., 2003, "A Split-Step Scheme for the Incompressible Navier-Stokes Equations," In: Hafez MM, (Ed.), Numerical Simulation of Incompressible Flow, World Scientific, pp. 108-125.

[16] Rahbar, E., Moli, D., and Moore, J., 2009, "Three-Dimensional Analysis of Flow Disturbances from Clots in Vena Cava Filters," J. Vasc. Interv. Radiol., 20(2), pp. S22.

[17] Cheng, C.P., Herfkens, R.J., and Taylor, C.A., 2003, "Inferior Vena Cava Hemodynamics Quantified In Vitro at Rest and During Cyclic Exercise Using Magnetic Resonance Imaging," Am. J. Physiol. Heart Circ. Physiol, 284, 1161-1167.

[18] Sadif, A., Rasuli, P., Olivier, A., Hadziomerovic, A., French, G.J., Aquino, J., O'Kelly, K., and Al-Mutairi, B., 2007, "Significant Caval Penetration by the Celect Inferior Vena Cava Filter: Attributable to Filter Design," J. Vasc. Interv. Radiol., 18, pp. 1447-1450.

[19] Harlal, A., Ojha, M., and Johnston, K.W., 2007, "Vena Cava Filter Performance Based on Hemodynamics and Reported Thrombosis and Pulmonary Embolism Patterns," J. Vasc. Interv. Radiol., 18, pp. 103-115.

[20] Ditenfass, L., 1964, "Rheological Approach to Thrombosis and Atherosclerosis," Angiology, 15, pp. 333-343.

[21] Schoephoerster, R.T., Oynes, F., Nunez, G., Kapadvanjwala, M., and Dewanjee, M.K., 1993, "Effects of Local Geometry and Fluid Dynamics on Regional Platelet Deposit on Artificial Surfaces," Arterioscler. Thromb., 13, pp. 1806-1813.

[22] Iqbal, S.I., Dave, B., Walker, G., Wicky, S., and Kalva, S.P., 2009, "Factors Affecting Retrieval of Inferior Vena Cava Filters," J. Vasc. Interv. Radiol., 20(2), pp. S24-S25.

[23] Smouse, H.B., Van Alstine, W.G., Mack, S., McCann-Brown, J.A., 2009, "Deployment Performance and Retrievability of the Cook Celect Vena Cava Filter," J. Vasc. Interv. Radiol., 20(3), pp, 375-383.

[24] Doody, O., Given, M.F., Kavnoudias, H., Street, M., Thomson, K.R., and Lyon, S.M., 2009, "Initial Experience in 115 Patients with the Retrievable Cook Celect Vena Cava Filter," J. Med. Imaging Radiat. Oncol., 53(1), pp. 64-68.

[25] Davies, P.F., 2009, "Hemodynamic Shear Stress and the Endothelium in Cardiovascular Pathophysiology," Nat. Clin. Pract. Cardiovasc. Med., 6(1), pp. 16-26.

[26] Keynton, R.S., Evancho, M.M., Sims, R.L., Rodway, N.V., Gobin, A., and Rittgers, S.E., 2001, "Intimal Hyperplasia and Wall Shear in Arterial Bypass Graft Distal Anastomoses: An *In vivo* Model Study," J. Biomech. Eng., 123, pp. 464-473.

[27] Wang, H.Q., Huang, L.X., Qu, M.J., Yan, Z.Q., Liu, B., Shen, B.R., and Jiang, Z.L., 2006, "Shear Stress Protects Against Endothelial Regulation of Vascular Smooth Muscle Cell Migration in a Coculture System," Endothelium, 13, pp. 171-180.

[28] Looby, S., Given, M.F., Geoghegan, T., McErlean, A., and Lee, M.J., 2007, "Günther Tulip Retrievable Inferior Vena Caval Filters: Indications, Efficacy, Retrieval, and Complications," Cardiovasc. Intervent. Radiol., 30(1), pp. 59-65.

Conflict of interest statement

The authors declare no conflicts of interest.